Wu *et al. Biochar* (2026) 8:89
https://doi.org/10.1007/s42773-026-00590-3

Biochar

ORIGINAL RESEARCH Open Access

Titanium dioxide-loaded biochar composite simultaneously reduces arsenic mobilization and methane emissions in flooded paddy soils

Song Wu[1], Zhiyuan Zhu[1,2], Dunfeng Si[3], Chuang Zhao[4], Hai Feng[1], Qian Zhang[1,5], Juan Wang[5], Dongmei Zhou[3] and Yujun Wang[1*]

Abstract

Arsenic (As) contamination and methane emissions from flooded paddy soils pose persistent challenges to food safety and environmental sustainability. Biochar-based amendments have attracted increasing attention for their capacity to regulate soil redox processes and associated biogeochemical cycling; however, achieving simultaneous mitigation of arsenic mobilization and methane emissions remains challenging. In this study, we developed a titanium dioxide (TiO_2)-loaded biochar composite and evaluated its effectiveness in controlling As mobilization and methane production in flooded paddy soil. The TiO_2-loaded biochar composite exhibited superior adsorption capacity for arsenite [As(III)] compared with arsenate [As(V)], even in the presence of competing anions. In laboratory assays, the composite effectively captured As(III) released during microbial reduction of ferrihydrite by *Shewanella oneidensis* MR-1, while As(V) immobilization remained largely unchanged. When applied to flooded paddy soils, the composite significantly reduced dissolved organic matter (DOM) concentrations, thereby disrupting its dual role as an electron shuttle and microbial carbon source. This reduction suppressed Fe(III) reduction and subsequent As mobilization. Under methanogenic and sulfate-reducing conditions, where pore-activated biochar showed limited effect, TiO_2-loaded biochar composite decreased porewater As concentrations by 88.3% over 30 days and substantially inhibited methane emissions. These results demonstrate that the TiO_2-loaded biochar composite can simultaneously mitigate As mobilization and methane production by combining high As(III) affinity with redox-mediated regulation of soil microbial processes.

Highlights

- Ti-PABC efficiently adsorbed As(III) in solutions with competing anions.
- Ti-PABC adsorbed As(III) but not As(V) during microbial reduction of As(III)-bearing ferrihydrite.
- Ti-PABC inhibited soil Fe(III) reduction by adsorbing DOM.
- Ti-PABC decreased soil As(III) and dimethylarsenate release at varied microbial niches.
- Ti-PABC mitigated soil methane emission by blocking DOM electron shuttling and competitive electron storage.

Keywords Paddy soil, Arsenic, Methane emission, Biochar, Titanium dioxide, Dissolved organic matter, Electron shuttle, Competitive electron acceptor

*Correspondence:
Yujun Wang
yjwang@issas.ac.cn
Full list of author information is available at the end of the article

© The Author(s) 2026. **Open Access** This article is licensed under a Creative Commons Attribution 4.0 International License, which permits use, sharing, adaptation, distribution and reproduction in any medium or format, as long as you give appropriate credit to the original author(s) and the source, provide a link to the Creative Commons licence, and indicate if changes were made. The images or other third party material in this article are included in the article's Creative Commons licence, unless indicated otherwise in a credit line to the material. If material is not included in the article's Creative Commons licence and your intended use is not permitted by statutory regulation or exceeds the permitted use, you will need to obtain permission directly from the copyright holder. To view a copy of this licence, visit http://creativecommons.org/licenses/by/4.0/.

Springer

Graphical Abstract

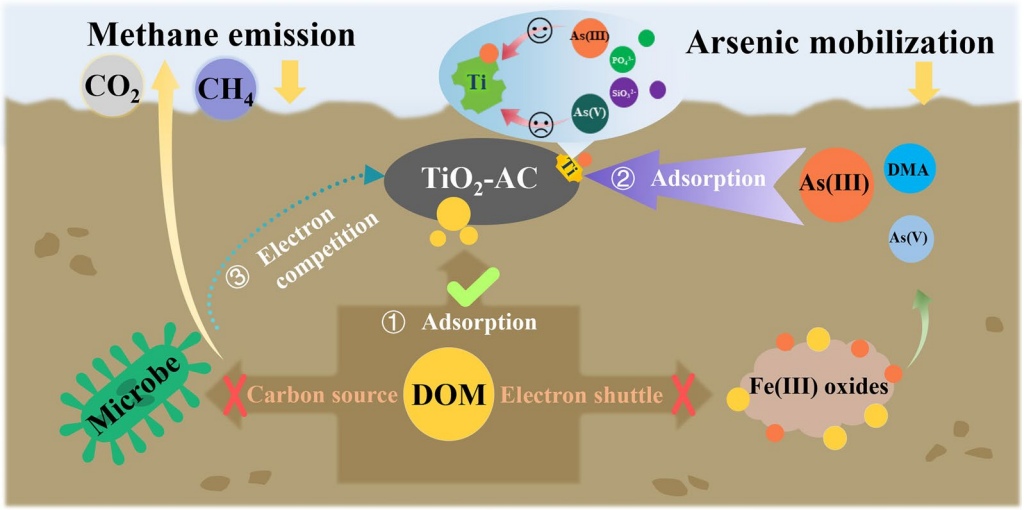

1 Introduction

Rice paddies, which cover ~ 9% of global cropland and feed over half the world's population, are characterized by intense water management and serve as a model system for studying soil biogeochemistry (Liu et al. 2021). Under flooding conditions, a succession of microbial niches develops, driven by the sequential utilization of electron acceptors such as nitrate, Mn(IV), Fe(III), and sulfate, ultimately leading to methane (CH_4) emission (Ge et al. 2024; Kögel-Knabner et al. 2010). Compounding this complexity, geogenic high background values of arsenic (As), along with ongoing human activities like mining, pesticide usage, and industrial emissions, have resulted in increasing As pollution in croplands worldwide (Hou et al. 2025; Zhang et al. 2024b).

In flooded paddy soils, the fate of As is intimately linked to key microbial processes. The reduction of arsenate (As(V)) to arsenite (As(III)), along with the methylation and thiolation of As species, is strongly coupled with Fe(III) reduction and sulfate reduction, respectively (Chen et al. 2019; Roberts et al. 2009). Furthermore, the demethylation of methylated As is associated with CH_4 production (Chen et al. 2023a). These processes, together with efficient root uptake of inorganic As and foliar translocation of methylated As to grains, lead to higher As accumulation in rice than in other cereals, threatening yield and safety (Gao et al. 2024; Wang et al. 2025; Williams et al. 2007). Rice paddies are also a major source of greenhouse gases, contributing ~ 48% of cropland emissions, with CH_4 emission alone accounting for 63.5% of rice's carbon footprint (Qian et al. 2023; Xia et al. 2023). The close linkage between As biogeochemistry and methanogenesis suggests the potential for co-managing As contamination and CH_4 emissions.

Electron competition strategies, which leverage the sequential utilization of electron acceptors during anaerobic decomposition, have been proposed to mitigate both As mobilization and CH_4 emission. Introducing oxygen into the plow layer through intermittent irrigation (Yang et al. 2025), embedded oxygen-permeable silicone tubes (Yuan et al. 2023a, 2023b), or amendments like calcium peroxide and oxygen nanobubbles (Chen et al. 2023b; Sha et al. 2020; Syu et al. 2020), has proven effective. Biochar, containing redox-active functional groups and a conductive carbon matrix, can function as an electron shuttle or a competitive electron acceptor in anaerobic biogeochemical redox reactions (Sun et al. 2017; Wu et al. 2017). While it can mitigate CH_4 emissions by acting as a competitive electron acceptor (Nan et al. 2025; Sun et al. 2021; Xin et al. 2023), biochar also facilitates Fe(III) reduction as an electron shuttle (Kappler et al. 2014), thereby mobilizing As (Wang et al. 2017; Wu et al. 2018). Notably, Fe(III) (oxyhydr)oxides serve not only as a dominant electron acceptor in anaerobic respiration but also play a key role in As immobilization in flooded soil (Aeppli et al. 2022; Keiluweit et al. 2017; Roberts et al. 2009). Therefore, modifying biochar to regulate Fe(III) reduction and As release, or to enhance As adsorption under flooding, is essential for simultaneously addressing As contamination and CH_4 emissions.

While loading Fe(III) minerals onto biochar enhances its As adsorption capacity (Wang et al. 2015), this benefit

is compromised by the reductive dissolution of Fe(III) minerals, leading to As release (Wang and Shang 2025; Wu et al. 2018; Yin et al. 2017). An alternative approach involves modifying biochar with a pore activator to produce pore-activated biochar, which can suppress Fe(III) reduction and associated As release (Si et al. 2024; Zhang et al. 2024a). Nevertheless, its effectiveness in suppressing As release declines when the microbial niche shifts from Fe(III) reduction to sulfate reduction and methanogenesis. In contrast to Fe(III) minerals, titanium dioxide (TiO_2) is an effective As adsorbent that remains stable under reducing conditions (Duan et al. 2024; Luo et al. 2018). Loading TiO_2 on pore-activated biochar improves particle dispersion and enhances As removal efficiency (Jing et al. 2012). Nevertheless, sulfate-reducing bacteria can reduce As(V) adsorbed onto TiO_2, promoting the release of the more mobile As(III) (Luo et al. 2013, 2017). Therefore, a comprehensive investigation into the effectiveness of TiO_2-loaded biochar composite in preventing As(III) release throughout the entire flooding period is essential for developing reliable remediation strategies for As-contaminated paddy fields.

In this study, TiO_2-loaded biochar composite was fabricated and evaluated for its capacity to adsorb As under anaerobic conditions in the presence of co-occurring anions. Subsequently, the fate of As was appraised during the microbial reduction of As-bearing ferrihydrite mediated by TiO_2-loaded biochar composite. Finally, the material was applied to a flooded paddy soil to elucidate its influence on the dissolution and transformation of As, as well as on CH_4 emissions, throughout the shift in microbial niches from Fe(III) reduction to sulfate reduction and methanogenesis. The findings of this study contribute to the screening of agronomically applicable adsorbent-modified biochar composite for remediating As-contaminated rice paddies with low carbon emissions.

2 Materials and methods

2.1 Preparation of TiO_2-loaded biochar composite and arsenic-bearing ferrihydrite

For the preparation of TiO_2-loaded biochar with high specific surface area, the material was not directly derived from agricultural biomass and chemical activation. Instead, it was synthesized via direct pyrolysis of a mixture of commercially available pore-activated biochar (activated carbon, CAS 7440-44-0, Sigma-Aldrich) and a titanium precursor (titanium sulfate, CAS 12693-11-3, Sinopharm, see Text S1 in the Supporting Information). Specifically, 1, 2, or 4 g of titanium sulfate was dissolved in 10 mL of Milli-Q water, followed by the addition of 4 g of pore-activated biochar powder. The resulting mixture was ultrasonicated for 4 h, oven-dried at 100 °C, ground into a fine powder, and subsequently calcined in a muffle furnace at 500 °C for 4 h to obtain the TiO_2-loaded biochar composite. The resulting TiO_2-loaded biochar composites, prepared with initial titanium sulfate to pore-activated biochar mass ratios of 0:4, 1:4, 2:4, and 4:4, were designated as PABC, Ti-PABC-1, Ti-PABC-2, and Ti-PABC-3, respectively. After synthesis, the TiO_2-loaded biochar composites were washed and dried for further use. Their physicochemical properties were characterized using X-ray diffraction (XRD; Ultima IV, Rigaku, Japan), specific surface area analysis (Micromeritics ASAP2020, USA), and scanning electron microscopy with energy-dispersive X-ray spectroscopy (SEM–EDX; Sigma 500, Zeiss, Germany). A wet-chemical method was employed to assess the electron donating and accepting capacities of the TiO_2-loaded biochar composites, using ferricyanide as the oxidant and Ti(III) citrate as the reductant (Si et al. 2023).

Arsenate- and arsenite-bearing ferrihydrite (As(V)-FH and As(III)-FH) were synthesized by mixing 1 M $Fe(NO_3)_3$ with either 4.66 g L^{-1} $Na_2HAsO_4{\cdot}7H_2O$ or 1.94 g L^{-1} $NaAsO_2$ under continuous stirring at 600 rpm. A 1 M KOH solution was added dropwise to adjust the pH to 7.5. The resulting precipitate was collected by centrifugation at 4000 rpm, washed repeatedly with Millipore water to remove soluble ions, and then resuspended in water to achieve a final Fe(III) concentration of 400 mM. The calculated As concentration in the As(V)-FH or As(III)-FH suspension was 400 mg L^{-1}, although the actual value was likely lower due to As desorption during the preparation and washing processes. The suspension was purged with nitrogen gas and stored in serum bottles until use.

2.2 Anoxic adsorption of arsenate and arsenite by TiO_2-loaded biochar composite

Given that biochar can oxidize As(III) under oxic conditions across a range of pH levels (Si et al. 2023; Zhu et al. 2022), adsorption experiments were conducted under anoxic conditions in 50 mL Corning tubes inside a glovebox (Etelux Lab2000, China). Specifically, 1 g L^{-1} of adsorbent (PABC, Ti-PABC-1, Ti-PABC-2, and Ti-PABC-3) and 10 mg L^{-1} of As(III) or As(V) were spiked to Millipore water or to solutions containing 10 mM PO_4^{3-} or 10 mM SiO_3^{2-}, with a final volume of 40 mL. After rotating at 80 rpm for 5 h in the glovebox, the filtrate was collected and analyzed for dissolved As concentration using atomic fluorescence spectrometry (AFS-230E, Haiguang, China).

2.3 Microbial reduction of arsenic-bearing ferrihydrite mediated by TiO_2-loaded biochar composite

The experiment investigating the microbial reduction of As(V)-FH or As(III)-FH mediated by TiO_2-loaded biochar composites was conducted in 100 mL serum bottles. The medium contained the iron-reducing bacterium *Shewanella oneidensis* MR-1, an adsorbent (PABC, Ti-PABC-1, Ti-PABC-2, and Ti-PABC-3) at 1 or 2 g L^{-1}, 10 mM either As(III)-FH or As(V)-FH (with As concentration less than 10 mg L^{-1}), 10 mM sodium lactate, and an anaerobic mineral medium (0.6 g L^{-1} KH_2PO_4, 0.3 g L^{-1} NH_4Cl, 0.5 g L^{-1} $MgSO_4{\cdot}7H_2O$, 0.1 g L^{-1} $CaCl_2{\cdot}2H_2O$, and 30 mM $NaHCO_3$). The pH of the medium was buffered at 7.00. *Shewanella oneidensis* MR-1 was first cultured in Luria–Bertani medium for 16 h. Bacterial cells were then harvested by centrifugation, washed, and resuspended in an equal volume of anaerobic mineral medium. The anaerobic cultivation was initiated by inoculating 1 mL of this bacterial suspension or, for abiotic controls, 1 mL of Millipore water. Each treatment was performed in 3–6 replicates, and all serum bottles were incubated in the dark at 28 °C with shaking at 150 rpm.

Samples were collected at specified intervals using a syringe. For whole Fe(II) and Fe(III) analysis, 0.1 mL of the suspension was mixed with 0.9 mL of 1 M HCl for 1 h to determine ferrous and total iron content. For aqueous-phase analysis, approximately 0.2 g of filtrate was combined with 0.8 mL of 1 M HCl to measure dissolved Fe^{2+}, As(III), and As(V) concentrations. Entire serum bottles were sacrificially sampled at 120, 332, and 774 h to characterize the mineralogical composition, morphology, and elemental distribution of the solid precipitates.

2.4 Anaerobic soil microcosm incubation with the application of TiO_2-loaded biochar composite

An As-contaminated paddy soil was collected from a mining area in Shangyu, Zhejiang, China. The soil was air-dried and sieved through a 20-mesh sieve, with total As and total iron content of 81.0 mg kg^{-1} and 21.7 g kg^{-1}, respectively. An anaerobic soil microcosm incubation was set up in 100 mL serum bottles containing 30 g of soil and 60 mL of Millipore water, with or without the addition of 0.3 g of PABC or Ti-PABC-1. A parallel incubation was conducted to monitor greenhouse gas emissions, using bottles containing 15 g of soil, 30 mL of Millipore water, and 0.15 g of PABC or Ti-PABC-1. All serum bottles were purged with nitrogen gas for 30 min to establish anoxic conditions, sealed with butyl rubber stoppers, and incubated statically in the dark at 28 °C.

At predetermined times, soil slurry, porewater, and gas samples were collected inside a glovebox. Specifically, 0.5 mL of slurry was mixed with 0.5 mL of 2 M anoxic HCl and extracted for 5 h to quantify low-crystalline iron. Porewater was filtered through a 0.45 μm membrane for analysis of dissolved As, iron, and dissolved organic carbon (DOC). Following gas sampling, serum bottles were opened in the glovebox, and the headspace was replenished with nitrogen in the antechamber before being resealed and returned to the incubator. Ferrous and total iron were measured using a microplate reader (HBS-1096A, Nanjing Defei Biotechnology Co., Ltd., China). CO_2 and CH_4 concentrations were analyzed by gas chromatography (7890A, Agilent Technologies, Inc., USA). Dimethylarsenate (DMA) in the porewater was quantified using high-performance liquid chromatography-inductively coupled plasma mass spectrometry (HPLC-ICP-MS, PerkinElmer NexION 2000, USA).

2.5 Chemical composition and electron shuttling capacity of dissolved organic matter

Following the anaerobic soil microcosm incubation at 30 days, anaerobically released DOM was extracted from the soil slurry inside a glovebox. The anaerobically released DOM solutions derived from the control, PABC, and Ti-PABC-1 treatments were designated as DOM-CK, DOM-PABC, and DOM-Ti-PABC-1, respectively. Additionally, fresh DOM (DOM-fresh) was extracted from the initial dry soil at a soil-to-water ratio of 1:2. After shaking for 30 min (28 °C, 150 rpm), the solution was filtered through a 0.45 μm membrane. The total organic carbon content of the DOM solutions was quantified using a TOC analyzer (Vario TOC cube, Elementar, Germany), while their fluorescence characteristics were assessed by excitation–emission matrix (EEM) spectroscopy (Hitachi F-7000, Japan).

To evaluate the electron shuttling capacity of the anaerobically released and freshly extracted DOM samples, a microbial ferrihydrite reduction assay was performed. An As-free ferrihydrite was synthesized as described previously. The experiment was conducted in 20 mL of anaerobic mineral medium containing 10 mM sodium lactate, 10 mL of DOM solution, 10 mM ferrihydrite, and *S. oneidensis* MR-1. Mineral suspensions were sampled at predetermined time intervals for the measurement of Fe(II) and total Fe concentrations.

3 Results and discussion

3.1 TiO_2-loaded biochar composite efficiently adsorbs arsenite at anion co-occurred anoxic solutions

The XRD spectra of PABC, Ti-PABC-1, Ti-PABC-2, and Ti-PABC-3 confirmed the successful loading of TiO_2, as evidenced by distinct anatase characteristic peaks at 25.3°, 37.8°, 48°, 53.9°, and 55.1° (Fig. 1a). The specific surface area, total pore volume, and micropore volume of the composites decreased with increasing TiO_2 loading (Figs. 1b, c, Table 1). SEM images showed no large TiO_2

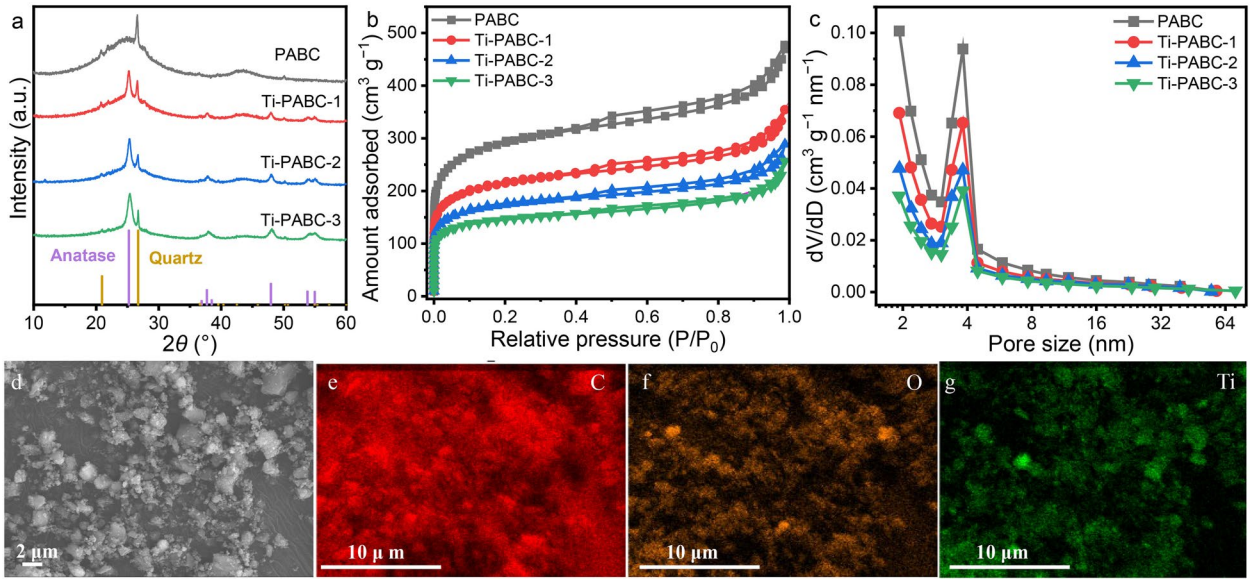

Fig. 1 Structural and morphological characterization of the adsorbents. X-ray diffraction patterns (**a**), nitrogen sorption–desorption isotherms (**b**), and micropore-mesopore pore size distribution curves (**c**) of pore-activated biochar (PABC) and titanium dioxide-loaded biochar composites (Ti-PABC-1, Ti-PABC-2, and Ti-PABC-3). Scanning electron microscopy image of Ti-PABC-3 (**d**) and the corresponding energy dispersive X-ray spectroscopy elemental mappings for carbon (**e**), oxygen (**f**), and titanium (**g**)

Table 1 Material properties and arsenic immobilization performance. Specific surface area, total pore volume, micropore volume, titanium content, and electron donating and electron accepting capacities (EDC and EAC) of pore-activated biochar (PABC) and titanium dioxide-loaded biochar composites (Ti-PABC-1, Ti-PABC-2, and Ti-PABC-3)

Sample	BET ($m^2\ g^{-1}$)	Total pore volume ($cm^3\ g^{-1}$)	Micropore volume ($cm^3\ g^{-1}$)	Ti loading rate ($g\ g^{-1}$)	EAC	EDC	As(III) adsorbed (mg g^{-1})			As(V) adsorbed (mg g^{-1})		
					mmol	$e^-\ g^{-1}$	H_2O	PO_4^{3-}	SiO_3^{2-}	H_2O	PO_4^{3-}	SiO_3^{2-}
PABC	1085	0.739	0.405	-	1.77	0.113	0.1717			0.111		
Ti-PABC-1	801	0.549	0.311	0.046	1.86	0.021	2.97	2.71	2.22	4.13	1.01	1.07
Ti-PABC-2	639	0.447	0.231	0.085	1.67	0.091	4.43			6.59		
Ti-PABC-3	539	0.397	0.182	0.148	1.47	0.072	6.04	5.82	5.09	8.27	0.84	1.03

The sum of EAC and EDC is electron exchange capacity. The arsenite (As(III)) and arsenate (As(V)) immobilization capacities were determined in Millipore water, 10 mM phosphate, or 10 mM silicate solutions at pH 7.00

aggregates on Ti-PABC-1, Ti-PABC-2, and Ti-PABC-3 (Figs. S1a–c, Fig. 1d). Furthermore, SEM–EDX elemental mapping demonstrated the uniform distribution of TiO_2 on Ti-PABC-3 particles (Figs. 1d–g, Fig. S1d). The TiO_2-loaded biochar composites showed electron accepting capacities of 1.47–1.77 mmol $e^-\ g^{-1}$, with electron donating capacities in the range of 0.021–0.113 mmol $e^-\ g^{-1}$. A slight decrease in electron exchange capacity was observed with increasing TiO_2 loading.

At pH 7.00, As(III) exists predominantly as neutral H_3AsO_3 molecules, whereas As(V) is present as $H_2AsO_4^-$ and $HAsO_4^{2-}$ anions. The TiO_2-loaded biochar composites exhibited higher adsorption capacities for As(V) than for As(III) in Millipore water. Specifically, the As(III) adsorption capacities of Ti-PABC-1, Ti-PABC-2, and Ti-PABC-3 were 2.97, 4.43, and 6.04 mg g^{-1}, respectively, while their corresponding As(V) adsorption capacities reached 4.13, 6.59, and 8.27 mg g^{-1} (Table 1). This observation underscores the importance of developing methods to oxidize As(III) to As(V) for enhanced removal (Duan et al. 2024; Fang et al. 2024).

Notably, the presence of competing anions significantly influenced As adsorption. Coexisting phosphate and silicate reduced the As(V) adsorption capacity of the TiO_2-loaded biochar composites by 74.1–89.9%, whereas the reduction for As(III) was only 3.64–25.3%. This finding aligns with previous studies, which reported higher As(III) removal efficiency than As(V)

on TiO_2 in anion-rich solution (Cui et al. 2015; Hu et al. 2015; Jegadeesan et al. 2010). On the one hand, this can be attributed to the similar dissociation constants between H_3AsO_3 (pK_a 9.22) and H_2SiO_3 (pK_a 9.77), as well as between H_3AsO_4 (pK_{a1} 2.2, pK_{a2} 6.98) and H_3PO_4 (pK_{a1} 2.12, pK_{a2} 7.2), leading to stronger competition for As(V) adsorption sites (Yan et al. 2016). On the other hand, the adsorption of As(III) on materials-loading TiO_2 showed higher resist to competing anions than that on pure TiO_2 (Niu et al. 2009). From a soil chemistry perspective, inhibiting the release of As(III) under flooded conditions is key to preventing As contamination (Zhao and Wang 2020). These results collectively demonstrate the applicability of TiO_2-loaded biochar composite for efficient As(III) removal in reducing environments with coexisting anions.

3.2 TiO_2-loaded biochar composite alleviates arsenite release while facilitating microbial reduction of As-bearing ferrihydrite as an electron shuttle

During *S. oneidensis* MR-1 reduction of As(V)-FH, the addition of PABC and Ti-PABC-2 increased the Fe(II) generation rate from 0.071 mmol L^{-1} h^{-1} to 0.346 and 0.345 mmol L^{-1} h^{-1}, respectively (Fig. 2a). This was in accordance with the previous studies that PABC and biochar were electron shuttles for facilitating *S. oneidensis* MR-1 reduction of ferrihydrite (Kappler et al. 2014; Wu et al. 2017). The accelerated ferrihydrite reduction promoted the immobilization of dissolved As(V) (Fig. 2b), with no significant difference observed between PABC and Ti-PABC-2. In abiotic controls, PABC and Ti-PABC-2 did not significantly alter dissolved As concentrations compared to the control (Fig. 2b). Phosphate and bicarbonate were present at 4.41 and 30 mM in the culture medium, respectively, which are the main competing

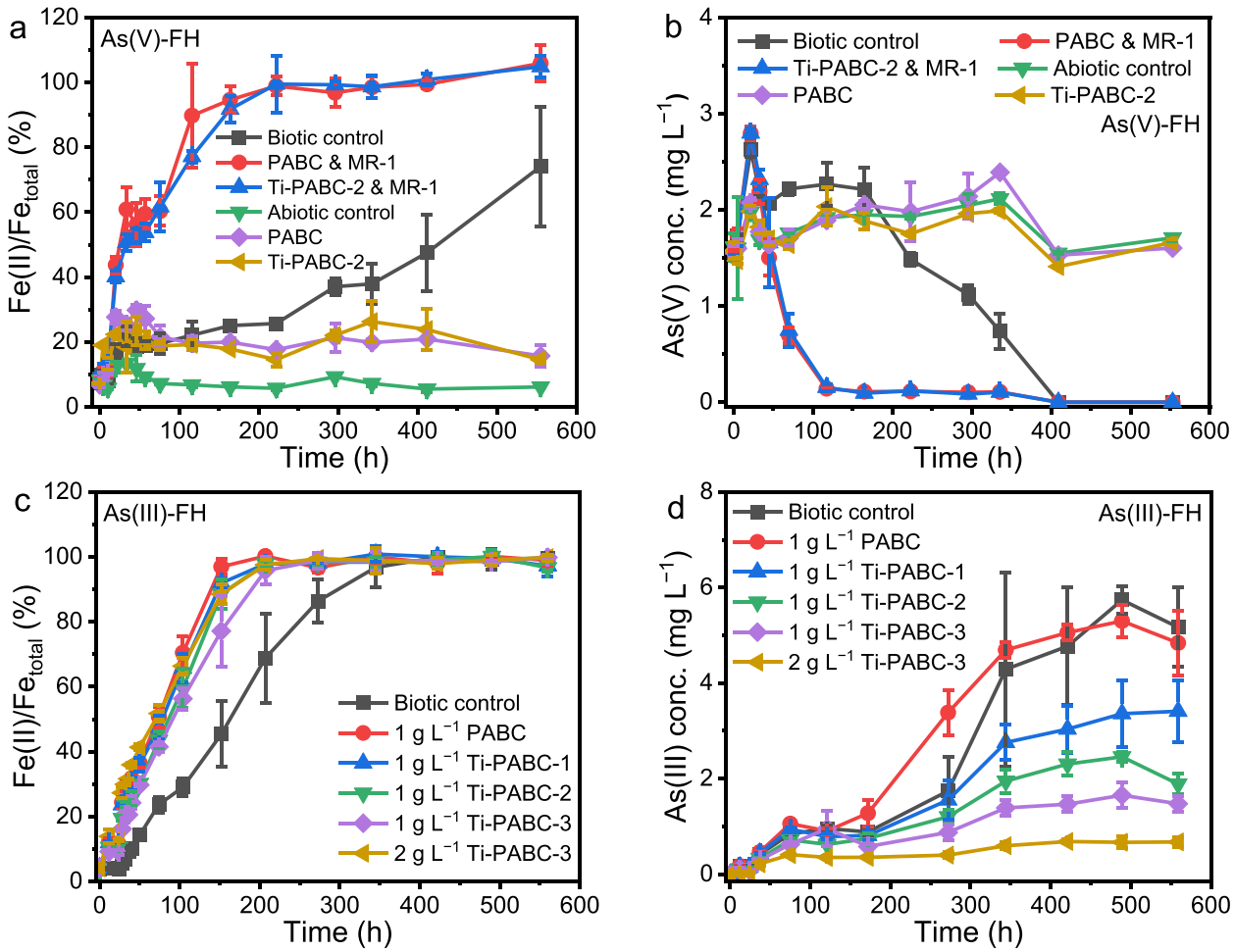

Fig. 2 Temporal changes in suspension Fe(II) percentage (**a**, **c**) and filtrate dissolved arsenic concentrations (**b**, **d**) during the reduction of arsenate-bearing (As(V)-FH, **a**, **b**) or arsenite-bearing (As(III)-FH, **c**, **d**) ferrihydrite in the absence and presence of pore-activated biochar (PABC) and titanium dioxide-loaded biochar composites (Ti-PABC-1, Ti-PABC-2, and Ti-PABC-3)

anions for As(V) adsorption (Deng et al. 2010). This explained the insignificant adsorptive removal of As(V) with the addition of Ti-PABC-2.

During *S. oneidensis* MR-1 reduction of As(III)-FH, both PABC and TiO_2-loaded biochar composites enhanced Fe(II) production. However, higher TiO_2 loading resulted in a slower Fe(II) production rate (Fig. 2c), as reflected in the reduced electron shuttling efficiency for ferrihydrite reduction. This decrease can be explained by the combined effect of a lower electron exchange capacity and impeded electron transfer due to TiO_2 coverage. Increasing the Ti-PABC-3 dosage from 1 to 2 g L^{-1} further elevated the Fe(II) generation rate (1.10 vs. 0.597 mmol L^{-1} h^{-1}). The absence of *S. oneidensis* MR-1 resulted in no significant release of As(III) or Fe^{2+} (Figs. S2a-c, SI). While PABC accelerated microbial reduction of ferrihydrite and promoted As(III) release (reaching 3.38 mg L^{-1} at 272 h compared to 1.74 mg L^{-1} in the control), TiO_2-loaded biochar composites significantly suppressed As(III) release despite also facilitating Fe(III) reduction (Fig. 2d). A higher TiO_2 loading rate resulted in a slower As(III) release rate. At the end of the incubation, dissolved As(III) concentrations in the Ti-PABC-1 (3.41 mg L^{-1}), Ti-PABC-2 (1.89 mg L^{-1}), Ti-PABC-3 (1.48 mg L^{-1}), and 2 g L^{-1} Ti-PABC-3 (0.675 mg L^{-1}) treatments were all lower than those in the control (5.17 mg L^{-1}) and PABC (4.84 mg L^{-1}) treatments. This inhibition of As(III) release is likely attributable to the adsorption of As(III) by the loaded TiO_2.

3.3 Selective immobilization of arsenite in TiO_2-loaded biochar composite while facilitating microbial reduction of As-bearing ferrihydrite

During *S. oneidensis* MR-1 reduction of As(III)-FH and As(V)-FH, PABC and Ti-PABC-2 accelerated the sequential precipitation of vivianite and siderite but did not alter the types of secondary minerals formed (Figs. 3a, b). For As(III)-FH reduction, vivianite was detected earlier (120 h) in PABC and Ti-PABC-2 treatments compared to the control (322 h). By 774 h, both vivianite and siderite were present in all treatments, with stronger siderite peaks in the PABC and Ti-PABC-2 treatments. A similar pattern was observed for As(V)-FH reduction, with siderite formation occurring faster in the PABC treatment. No crystalline secondary minerals were detected in abiotic controls (Fig. S3, SI). The anatase peaks of Ti-PABC-2 remained unchanged throughout the incubation.

SEM–EDX analysis of solid precipitates from the As(III)-FH reduction after 774 h revealed flake-shaped minerals (>10 μm) and cubic-shaped minerals (3–5 μm)

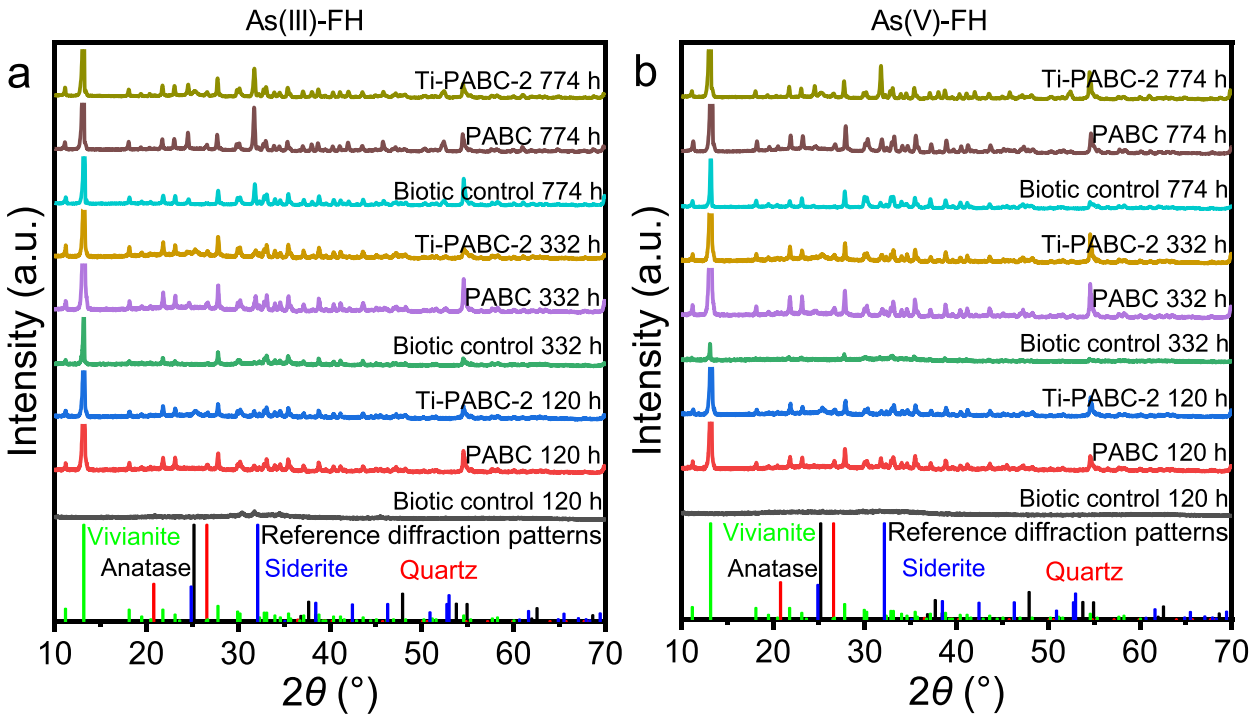

Fig. 3 X-ray diffractograms of solid phases collected at 120, 332, and 774 h. The patterns correspond to the reduction of arsenite-bearing (As(III)-FH **a**) and arsenate-bearing ferrihydrite (As(V)-FH **b**) by *Shewanella oneidensis* MR-1, conducted in the absence and presence of PABC or Ti-PABC-2, respectively

in the control (Fig. 4a). Elemental mapping identified the flakes as vivianite [$Fe_3(PO_4)_2$], containing Fe, P, and O (Figs. 4b–d), and the cubes as siderite ($FeCO_3$), containing Fe and O. The addition of PABC and Ti-PABC-2 caused the stacking of vivianite flakes and reduced the size of siderite crystals to below 0.5 μm (Figs. 4e–l). This accelerated Fe^{2+} release from enhanced ferrihydrite reduction (Fig. S2d, SI) likely promoted vivianite precipitation and stacking.

S. oneidensis MR-1 reduces Fe(III) in As(V)-FH but not As(V). Both PABC and Ti-PABC-2 promoted As(V) fixation during As(V)-FH reduction. SEM–EDX mapping showed As(V) enrichment in flake-shaped vivianite but not associated with Ti-PABC-2 or siderite (Fig. 5). EDX point scans confirmed a distinct As signal in vivianite but not in TiO_2-loaded biochar composite (Figs. 5g, h, S5, SI), consistent with known preferential immobilization of As(V) in vivianite over siderite (Muehe et al. 2013; Wu et al. 2018). Given Ti-PABC-2's negligible As(V) adsorption in the culture medium abiotically (Fig. 2b, SI), we conclude that vivianite formation was primarily responsible for As(V) immobilization.

In contrast, during As(III)-FH reduction, As(III) release in the control and PABC treatments indicated that neither vivianite nor siderite effectively immobilized As(III), consistent with previous findings (Wu et al. 2018). SEM–EDX mapping showed no significant accumulation of As(III) on Ti-PABC-2 particles (Fig. S6, SI). However, weak As signals were detected on Ti-PABC-2 particles by EDX point analysis, but not in vivianite (Fig. S7, SI). This was likely due to the uniform dispersion of TiO_2, low Ti content (0.085 g g^{-1} in Ti-PABC-2), and low As loading (< 4.43 mg g^{-1} in Ti-PABC-2) in the composite. In summary, TiO_2-loaded biochar composite served as an efficient electron shuttle for the microbial reduction of As-bearing ferrihydrite, the mitigated risk of As(V) was due to its immobilization in vivianite, while the reduced risk of As(III) was caused by adsorption onto the TiO_2-loaded biochar composite.

3.4 TiO_2-loaded biochar composite simultaneously mitigates As mobilization and CH_4 emissions

During the 30-day anaerobic soil incubation, both PABC and Ti-PABC-1 inhibited Fe(III) reduction, the release of dissolved Fe^{2+}, total As, As(III), DMA, and DOC, as well as the emissions of CO_2 and CH_4 (Fig. 6). The application of PABC and Ti-PABC-1 significantly reduced key parameters: the Fe(III) reduction rate decreased from 1.41 to 1.21 and 0.977 g kg^{-1} soil d^{-1}; the total As release rate dropped from 0.727 to 0.535 and 0.084 mg L^{-1} d^{-1}; and the DOC concentration declined from 152–176 to 69.7–71.6 and 79.9–93.2 mg

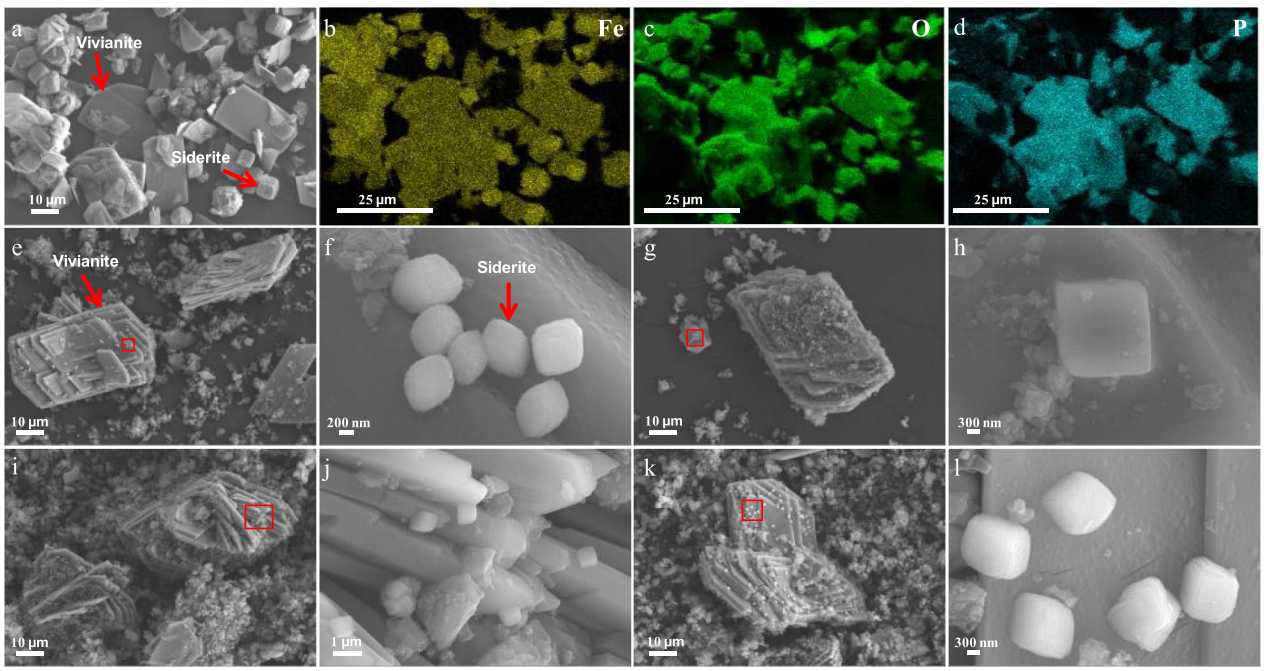

Fig. 4 Scanning electron microscopy with energy dispersive X-ray spectroscopy (SEM–EDX) characterization of the morphology and elemental distribution of secondary minerals formed during the microbial reduction of arsenic-bearing ferrihydrite. Images were obtained from experiments with no amendment (**a**–**d**), PABC (**e**, **f**, **i**, **j**), or Ti-PABC-2 (**g**, **h**, **k**, **l**), during the reduction of arsenite-bearing (**e**–**h**) or arsenate-bearing (**i**-**l**) ferrihydrite by *Shewanella oneidensis* MR-1. The areas within the red boxes in panels **e**, **g**, **i**, and **k** are shown at higher magnification in panels **f**, **h**, **j**, and **l**, respectively

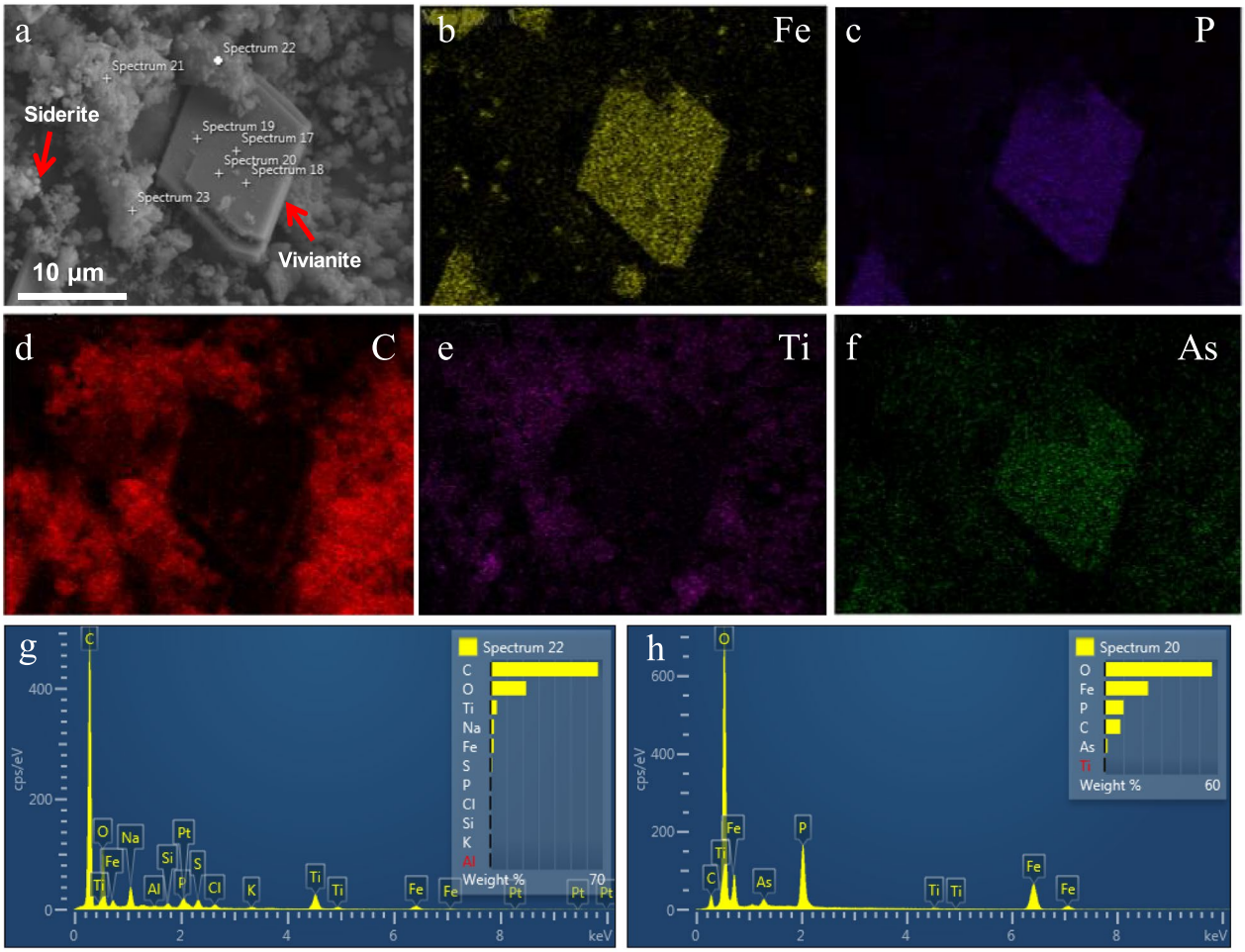

Fig. 5 Scanning electron microscopy with energy dispersive X-ray spectroscopy (SEM–EDX) characterization of the solid phase precipitates formed during the reduction of arsenate-bearing ferrihydrite by *Shewanella oneidensis* MR-1 in the presence of Ti-PABC-2. The figure shows the overall morphology (**a**) and the corresponding elemental distribution maps for Fe (**b**), P (**c**), C (**d**), Ti (**e**), and As (**f**). Panels (**g**) and (**h**) present the EDX spectra detailing the elemental composition at specific sites marked in the SEM image

L^{-1}, respectively. Although TiO_2 loading slightly weakened the inhibitory effect of PABC on Fe(III) reduction and DOC release, it significantly enhanced the suppression of As release throughout the incubation.

PABC initially inhibited As release primarily by delaying Fe(III) reduction. However, once soil Fe(II) content plateaued on day 30, PABC lost its effectiveness (porewater As: 4.86 vs. 5.33 mg L^{-1} in control), whereas Ti-PABC-1 continued to reduce As release by 88.3% on day 30. As(III) was the dominant species, constituting 53.3–105% of total porewater As (Fig. 6d). Both PABC and Ti-PABC-1 also decreased DMA concentrations. On day 6, before significant CH_4 emission, DMA concentrations were 11.5 and 7.86 µg L^{-1} in the control and Ti-PABC-1 treatments, respectively (Fig. 6e). By day 15, with the onset of significant methanogenesis, DMA concentrations decreased to 5.15 and 0.927 µg L^{-1}, likely due to demethylation by methanogens (Chen et al. 2023a).

The CO_2 emission rates were 2.17, 1.89, and 1.98 mmol kg^{-1} soil d^{-1}, and CH_4 emission rates were 1.68, 1.04, and 1.09 mmol kg^{-1} soil d^{-1} for the control, PABC, and Ti-PABC-1 treatments, respectively (Figs. 6g, h). Cumulative emissions from the control were 68.6 mmol CO_2 kg^{-1} and 42.2 mmol CH_4 kg^{-1}. PABC and Ti-PABC-1 reduced cumulative CO_2 emissions by 12.7% and 8.32%, and CH_4 emissions by 39.3% and 37.1%, respectively, with no significant difference between the two amendments.

3.5 Mechanism for reduced Fe(III) reduction, As mobilization, and CH_4 emissions by TiO_2-loaded biochar composite application in paddy soil

Biochar exhibits redox properties that enable it to serve as an electron shuttle and a competitive electron

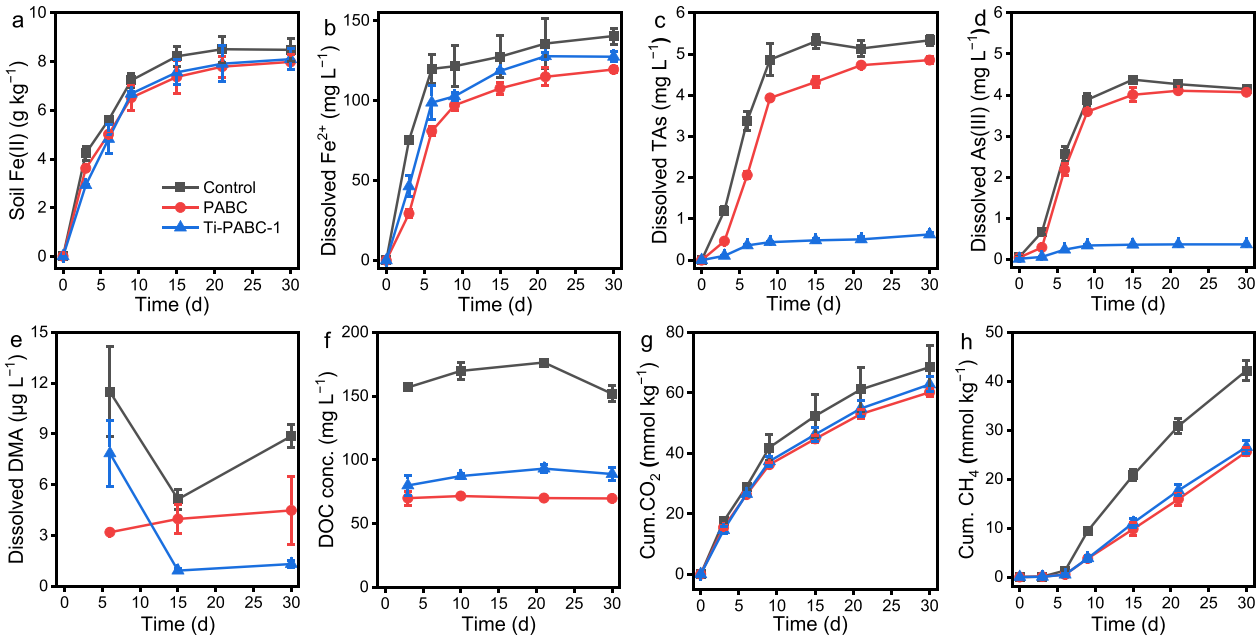

Fig. 6 Anoxic microcosm incubation of paddy soil amended with PABC or Ti-PABC-1. The panels display: 1 M HCl-extracted Fe(II) in the solid phase (**a**); dissolved ferrous ion concentration (**b**); solution-phase concentrations of total arsenic (TAs, **c**), arsenite (As(III), **d**), dimethylarsenate (DMA, **e**), and dissolved organic carbon (DOC, **f**); and cumulative emissions of carbon dioxide (CO_2, **g**) and methane (CH_4, **h**)

acceptor, thereby facilitating various anaerobic microbial respiration processes (Cornell et al. 2025; Hudson and Tratnyek 2025; Sun et al. 2017). Its electron-shuttling capability facilitates As release in paddy soils and sediments (Chen et al. 2016; Wang et al. 2017; Yang et al. 2022), rendering it unsuitable for controlling As contamination. PABC, as a pore-activated biochar, contains redox-active functional groups and conductive carbon matrix, allowing it to similarly serve as an electron shuttle (Wu et al. 2017, 2021). While PABC acted as an efficient electron shuttle to accelerate ferrihydrite reduction by *S. oneidensis* MR-1, it inhibited Fe(III) reduction in paddy soil. This contrasting behavior likely stems from the fact that both PABC and native soil DOM can shuttle electrons for soil Fe(III) reduction, whereas DOM was absent in the *S. oneidensis* MR-1 system (Bai et al. 2023; Wu et al. 2017).

Unlike biochar, microporous PABC and Ti-PABC-1 are strong DOM adsorbents. Their application reduced porewater DOC concentrations from 152–170 mg L^{-1} (control) to 69.7–71.6 mg L^{-1} (PABC) and 79.9–93.1 mg L^{-1} (Ti-PABC-1) (Fig. 6f). The DOM released under anaerobic conditions consisted mainly of humic-like and fulvic-like components (Figs. 7a–c). Both PABC and Ti-PABC-1 significantly reduced the fluorescence intensity of humic-like components, consistent with their higher affinity for high-molecular-weight humic substances (Ateia et al. 2017). Both the anaerobically released and freshly extracted DOM were effective electron shuttles for ferrihydrite reduction, with efficiency positively correlated with DOC concentration (Figs. 7e, f). DOM can diffuse through soil aggregates, enabling long-distance electron transfer via electron hopping (Bai et al. 2020, 2023), a capability not shared by non-diffusible PABC particles. Furthermore, freshly extracted DOM contained protein-like and soluble microbial byproduct-like components (Fig. 7d), which are readily biodegradable (Qiao et al. 2020; Yang et al. 2023; Zhou et al. 2018). The inhibition of Fe(III) reduction further restricted the release of mineral-associated organic matter for microbial utilization (Martens et al. 2023; Zhang et al. 2025). Therefore, sequestering DOM in PABC and Ti-PABC-1 not only inhibited its electron-shuttling function but also limited its role as a microbial carbon source, thereby delaying soil Fe(III) reduction and CO_2 emissions.

Once Fe(III) reduction stabilized, PABC alone did not significantly reduce As release into porewater. However, TiO_2-loaded biochar composite decreased As release, which could be ascribed to the adsorption on TiO_2. In contrast to the transient effect of PABC on total As, its sustained suppression of DMA release is attributed to the complex interplay between As methylation and demethylation under sulfate-reducing and methanogenic conditions, respectively (Dai et al. 2025). The role of redox-active biochar/PABC in methanogenesis is context-dependent. It can promote

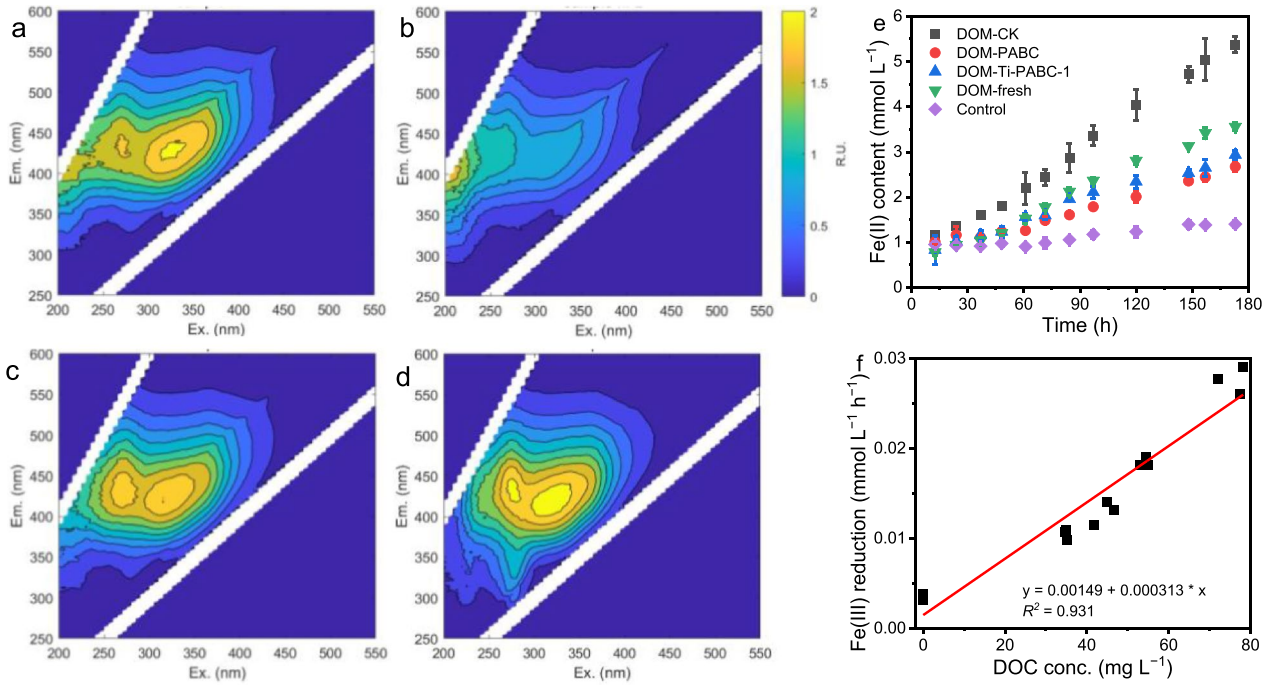

Fig. 7 Excitation-emission matrix (EEM) fluorescence spectra of dissolved organic matter (DOM) obtained from paddy soil under anoxic microcosm incubations on day 30 (DOM-CK **a**; DOM-PABC **b**; DOM-Ti-PABC-1 **c**) and from fresh soil (DOM-fresh **d**). Based on the EEM spectra, fluorescent components were categorized into four groups: humic-like (Ex 250–400 nm, Em 380–500 nm), fulvic-like (Ex 220–250 nm, Em 380–500 nm), protein-like (Ex 220–250 nm, Em 250–380 nm), and soluble microbial byproduct-like (Ex 250–400 nm, Em 250–380 nm). Electron shuttling efficiency of the extracted DOM in mediating ferrihydrite reduction by *Shewanella oneidensis* MR-1 (**e**). Correlation between DOM concentration and ferrihydrite reduction rate (**f**)

CH_4 production by facilitating direct interspecies electron transfer in microbial carbon source-rich environments, such as some anaerobic digestion systems (Chen et al. 2014; Liu et al. 2012; Xu et al. 2025) and methanogenic enrichment culture system of paddy soils (Yuan et al. 2018; Zhang et al. 2021). In contrast, it suppresses CH_4 production in microbial carbon source-limited environments like peat soils (Sun et al. 2021) and paddy soils (Nan et al. 2025; Si et al. 2024), as well as in some anaerobic digestion systems (Xin et al. 2023). The observed decrease in CH_4 emissions in this study can be explained by the limited supply of microbial carbon sources, delayed establishment of methanogenic niches (resulting from slower Fe(III) reduction), and electron competition from sulfate reduction and methanogenesis (i.e., competitive electron storage in electron-accepting functional groups of PABC) (Si et al. 2024; Sun et al. 2021; Xin et al. 2023). The comparable electron accepting capacity values of PABC and Ti-PABC-1 explain the negligible difference observed in soil CH_4 emissions (25.6 vs. 26.6 mmol CH_4 kg^{-1}).

4 Conclusions

This study presents a synergistic strategy that integrates the robust As(III) adsorption capacity of TiO_2 (even with competing anions present) with PABC's ability to inhibit soil Fe(III) reduction, As release and methylation, and CH_4 emissions. TiO_2-loaded biochar composite adsorbed As(III) more effectively than As(V) in anion-rich solutions. This resulted in reduced As(III) mobility but minimally affected As(V) fate during the PABC-promoted microbial reduction of As-bearing ferrihydrite. In flooded paddy soil, PABC delays Fe(III) reduction and As release by adsorbing DOM, thus suppressing DOM-driven electron shuttling. As microbial niches shift from Fe(III) reduction to sulfate reduction and methanogenesis, PABC alone becomes ineffective at curbing porewater As, while TiO_2-loaded biochar composite maintains strong suppression. Both materials effectively limited DMA release across these shifting microbial niches. Notably, TiO_2-loaded biochar composite also acted as a competitive electron acceptor, diverting electrons from methanogenesis and reducing CH_4 emissions. Since PABC's electron-shuttling role is

limited in soils, future work should prioritize its function as a competitive electron acceptor.

Controlling As pollution in paddies remains a critical challenge due to dynamic redox fluctuations, As mobility, and efficient rice uptake. Assessing adsorbent performance under different microbial niches provides a practical basis for material selection in remediation. Both commercial PABC and TiO_2 are readily available. However, the relatively high cost of PABC (3 to 10 times more expensive than unmodified biochar) limits its agricultural use. In contrast, the estimated low application rate (1725 kg ha^{-1}) and affordable price (approximately ¥10,000 per ton) of TiO_2 make it a more feasible option for field applications. To reduce overall material costs, either loading TiO_2 onto unmodified biochar or applying TiO_2 directly can be considered. Nevertheless, the remediation effectiveness of these alternative materials requires further evaluation. More importantly, besides short-term soil microcosm studies, long-term assessments are essential to examine the stability of these materials under alternating wet and dry cycles in paddy soils. Further pot and field trials remain crucial to verify the potential of these materials for simultaneously reducing As accumulation in rice grains and CH_4 emissions.

Supplementary Information

The online version contains supplementary material available at https://doi.org/10.1007/s42773-026-00590-3.

Supplementary Material 1

Acknowledgements
This work was supported by the National Natural Science Foundation of China (Grant Nos. 42225701 and 42477039).

Author contributions
Song Wu conceived the original idea; Dongmei Zhou and Yujun Wang supervised the project. Song Wu, Zhiyuan Zhu, Dunfeng Si, Dongmei Zhou, and Yujun Wang designed the experiments. Song Wu, Zhiyuan Zhu, Dunfeng Si, Hai Feng, and Qian Zhang performed the experiments and characterizations. Song Wu, Zhiyuan Zhu, Dunfeng Si, Chuang Zhao, Hai Feng, Qian Zhang, Juan Wang, Dongmei Zhou and Yujun Wang wrote and revised the paper. All authors commented on the paper.

Funding
National Natural Science Foundation of China, 42225701, Yujun Wang, 42477039, Song Wu.

Data availability
The data that support this study are available from the corresponding author upon request.

Declarations

Competing interests
Yujun Wang is an EBM of the journal Biochar, and he was not involved in the peer-review or handling of the manuscript. The authors declare no competing financial interests in this paper.

Author details
[1]State Key Laboratory of Soil and Sustainable Agriculture, Institute of Soil Science, Chinese Academy of Sciences, Nanjing 210008, China. [2]School of Environmental Science and Engineering, Suzhou University of Science and Technology, Suzhou, China. [3]State Key Laboratory of Pollution Control and Resource Reuse, School of Environment, Nanjing University, Nanjing 210023, China. [4]Shandong Institute of Geophysical and Geochemical Exploration, Jinan 250013, China. [5]School of Environmental and Municipal Engineering, North China University of Water Resources and Electric Power, Zhengzhou 450046, People's Republic of China.

Received: 11 June 2025 Revised: 4 February 2026 Accepted: 10 February 2026
Published online: 07 April 2026

References

Aeppli M, Thompson A, Dewey C, Fendorf S (2022) Redox properties of solid phase electron acceptors affect anaerobic microbial respiration under oxygen-limited conditions in floodplain soils. Environ Sci Technol 56(23):17462–17470

Ateia M, Apul OG, Shimizu Y, Muflihah A, Yoshimura C, Karanfil T (2017) Elucidating adsorptive fractions of natural organic matter on carbon nanotubes. Environ Sci Technol 51(12):7101–7110

Bai Y, Sun T, Angenent LT, Haderlein SB, Kappler A (2020) Electron hopping enables rapid electron transfer between quinone-/hydroquinone-containing organic molecules in microbial iron(III) mineral reduction. Environ Sci Technol 54(17):10646–10653

Bai Y, Sun T, Mansor M, Joshi P, Zhuang Y, Haderlein SB, Fischer S, Konhauser KO, Alessi DS, Kappler A (2023) Networks of dissolved organic matter and organo-mineral associations stimulate electron transfer over centimeter distances. Environ Sci Technol Lett 10(6):493–498

Chen S, Rotaru A-E, Shrestha PM, Malvankar NS, Liu F, Fan W, Nevin KP, Lovley DR (2014) Promoting interspecies electron transfer with biochar. Sci Rep. https://doi.org/10.1038/srep05019

Chen Z, Wang YP, Xia D, Jiang XL, Fu D, Shen L, Wang HT, Li QB (2016) Enhanced bioreduction of iron and arsenic in sediment by biochar amendment influencing microbial community composition and dissolved organic matter content and composition. J Hazard Mater 311:20–29

Chen C, Li LY, Huang K, Zhang J, Xie WY, Lu YH, Dong XZ, Zhao FJ (2019) Sulfate-reducing bacteria and methanogens are involved in arsenic methylation and demethylation in paddy soils. ISME J 13(10):2523–2535

Chen C, Li L, Wang Y, Dong X, Zhao F-J (2023a) Methylotrophic methanogens and bacteria synergistically demethylate dimethylarsenate in paddy soil and alleviate rice straighthead disease. ISME J 17:1851–1861

Chen G, Du Y, Fang L, Wang X, Liu C, Yu H, Feng M, Chen X, Li F (2023b) Distinct arsenic uptake feature in rice reveals the importance of N fertilization strategies. Sci Total Environ 854:158801

Cornell CR, Bangala JI, Masiello CA, Alvarez PJJ (2025) Beyond the bench: contextualizing the impacts of char redox properties on biogeochemical cycling and microbial ecosystem services. Environ Sci Technol 59(2):1080–1090

Cui J, Du J, Yu S, Jing C, Chan T (2015) Groundwater arsenic removal using granular TiO2: integrated laboratory and field study. Environ Sci Pollut Res 22(11):8224–8234

Dai J, Chen C, Zhai Z-Q, Gao A-X, Johnson DR, Kopittke PM, Zhao F-J, Wang P (2025) The balance between microbial arsenic methylation and demethylation in paddy soils underpins global arsenic risk and straighthead disease in rice. Proc Natl Acad Sci USA 122(38):e2508311122

Deng S, Li Z, Huang J, Yu G (2010) Preparation, characterization and application of a Ce–Ti oxide adsorbent for enhanced removal of arsenate from water. J Hazard Mater 179(1):1014–1021

Duan Y, Sun Y, Palomo A, Li Z, Yang B, Shi Q, Zhang DZ, Yang Q, Meng X, Zheng Y (2024) MnO_2-modified activated carbon and granular nano-TiO_2 in tandem succeed in treating domestic well water arsenic at point of use. Nat Water 2:674–683

Fang L, Liu K, Xu L, Wu F, Borch T, Li F (2024) Rechargeable carbonaceous geosupercapacitor for sustainable superoxide generation and pollutant abatement. Nat Water 2:485–495

Gao A-X, Chen C, Gao Z-Y, Zhai Z-Q, Wang P, Zhang S-Y, Zhao F-J (2024) Soil redox status governs within-field spatial variation in microbial arsenic methylation and rice straighthead disease. ISME J. https://doi.org/10.1093/ismejo/wrae057

Ge J, Wu S, Wu H, Lin J, Cai Y, Zhou D, Gu X (2024) Prediction of As and Cd dissolution in various soils under flooding condition. Sci Total Environ 948:174853

Hou D, Jia X, Wang L, McGrath SP, Zhu Y-G, Hu Q, Zhao F-J, Bank MS, O'Connor D, Nriagu J (2025) Global soil pollution by toxic metals threatens agriculture and human health. Science 388(6744):316–321

Hu S, Yan L, Chan T, Jing C (2015) Molecular insights into ternary surface complexation of arsenite and cadmium on TiO2. Environ Sci Technol 49(10):5973–5979

Hudson JM, Tratnyek PG (2025) Electrochemical characterization of pyrogenic carbons: implications for degradation of groundwater contaminants with carbon-based amendments. Environ Sci Technol 59(16):8283–8293

Jegadeesan G, Al-Abed SR, Sundaram V, Choi H, Scheckel KG, Dionysiou DD (2010) Arsenic sorption on TiO2 nanoparticles: size and crystallinity effects. Water Res 44(3):965–973

Jing C, Cui J, Huang Y, Li A (2012) Fabrication, characterization, and application of a composite adsorbent for simultaneous removal of arsenic and fluoride. ACS Appl Mater Interfac 4(2):714–720

Kappler A, Wuestner ML, Ruecker A, Harter J, Halama M, Behrens S (2014) Biochar as electron shuttle between bacteria and Fe(III) minerals. Environ Sci Technol Lett 1(8):339–344

Keiluweit M, Wanzek T, Kleber M, Nico P, Fendorf S (2017) Anaerobic microsites have an unaccounted role in soil carbon stabilization. Nat Commun 8(1):1771

Kögel-Knabner I, Amelung W, Cao Z, Fiedler S, Frenzel P, Jahn R, Kalbitz K, Kölbl A, Schloter M (2010) Biogeochemistry of paddy soils. Geoderma 157(1):1–14

Liu FH, Rotaru A-E, Shrestha PM, Malvankar NS, Nevin KP, Lovley DR (2012) Promoting direct interspecies electron transfer with activated carbon. Energy Environ Sci 5(10):8982–8989

Liu Y, Ge T, van Groenigen KJ, Yang Y, Wang P, Cheng K, Zhu Z, Wang J, Li Y, Guggenberger G, Sardans J, Penuelas J, Wu J, Kuzyakov Y (2021) Rice paddy soils are a quantitatively important carbon store according to a global synthesis. Commun Earth Environ 2(1):154

Luo T, Tian H, Guo Z, Zhuang G, Jing C (2013) Fate of arsenate adsorbed on nano-TiO_2 in the presence of sulfate reducing bacteria. Environ Sci Technol 47(19):10939–10946

Luo T, Ye L, Ding C, Yan JL, Jing CY (2017) Reduction of adsorbed As(V) on nano-TiO_2 by sulfate-reducing bacteria. Sci Total Environ 598(Supplement C):839–846

Luo T, Ye L, Chan T, Jing C (2018) Mobilization of arsenic on nano-TiO2 in soil columns with sulfate reducing bacteria. Environ Pollut 234:762–768

Martens J, Mueller CW, Joshi P, Rosinger C, Maisch M, Kappler A, Bonkowski M, Schwamborn G, Schirrmeister L, Rethemeyer J (2023) Stabilization of mineral-associated organic carbon in Pleistocene permafrost. Nat Commun 14(1):2120

Muehe EM, Scheer L, Daus B, Kappler A (2013) Fate of arsenic during microbial reduction of biogenic versus abiogenic As–Fe(III)–mineral coprecipitates. Environ Sci Technol 47(15):8297–8307

Nan Q, Speth DR, Qin Y, Chi W, Milucka J, Gu B, Wu W (2025) Biochar application using recycled annual self straw reduces long-term greenhouse gas emissions from paddy fields with economic benefits. Nat Food 6(5):456–465

Niu HY, Wang JM, Shi YL, Cai YQ, Wei FS (2009) Adsorption behavior of arsenic onto protonated titanate nanotubes prepared via hydrothermal method. Microporous Mesoporous Mater 122(1):28–35

Qian H, Zhu X, Huang S, Linquist B, Kuzyakov Y, Wassmann R, Minamikawa K, Martinez-Eixarch M, Yan X, Zhou F, Sander BO, Zhang W, Shang Z, Zou J, Zheng X, Li G, Liu Z, Wang S, Ding Y, van Groenigen KJ, Jiang Y (2023) Greenhouse gas emissions and mitigation in rice agriculture. Nat Rev Earth Env 4(10):716–732

Qiao W, Guo H, He C, Shi Q, Xiu W, Zhao B (2020) Molecular evidence of arsenic mobility linked to biodegradable organic matter. Environ Sci Technol 54(12):7280–7290

Roberts LC, Hug SJ, Dittmar J, Voegelin A, Kretzschmar R, Wehrli B, Cirpka OA, Saha GC, Ashraf Ali M, Badruzzaman ABM (2009) Arsenic release from paddy soils during monsoon flooding. Nat Geosci 3:53

Sha Z, Chen Z, Feng Y, Xue L, Yang L, Cao L, Chu Q (2020) Minerals loaded with oxygen nanobubbles mitigate arsenic translocation from paddy soils to rice. J Hazard Mater 398:122818

Si DF, Wu HT, Yang M, Fan TT, Wang DJ, Chen L, Zhu CY, Fang GD, Wu S, Zhou DM (2023) Linking pyrogenic carbon redox property to arsenite oxidation: impact of N-doping and pyrolysis temperature. J Hazard Mater 445:130477

Si DF, Wu S, Wu HT, Wang DJ, Fu Q-l, Wang YJ, Wang P, Zhao F-j, Zhou DM (2024) Activated carbon application simultaneously alleviates paddy soil arsenic mobilization and carbon emission by decreasing porewater dissolved organic matter. Environ Sci Technol 58(18):7880–7890

Sun TR, Levin BDA, Guzman JJL, Enders A, Muller DA, Angenent LT, Lehmann J (2017) Rapid electron transfer by the carbon matrix in natural pyrogenic carbon. Nat Commun 8:14873

Sun TR, Guzman JJL, Seward JD, Enders A, Yavitt JB, Lehmann J, Angenent LT (2021) Suppressing peatland methane production by electron snorkeling through pyrogenic carbon in controlled laboratory incubations. Nat Commun 12(1):4119

Syu CH, Yu CH, Lee DY (2020) Effect of applying calcium peroxide on the accumulation of arsenic in rice plants grown in arsenic-elevated paddy soils. Environ Pollut 266:115140

Wang Y, Shang J (2025) Iron (hydr)oxide-enriched biochar for arsenic immobilization under microbial iron reduction and fluctuating redox conditions. ACS ES&T Engin 5(7):1809–1820

Wang SS, Gao B, Zimmerman AR, Li YC, Ma L, Harris WG, Migliaccio KW (2015) Removal of arsenic by magnetic biochar prepared from pinewood and natural hematite. Bioresour Technol 175:391–395

Wang N, Xue X-M, Juhasz AL, Chang Z-Z, Li H-B (2017) Biochar increases arsenic release from an anaerobic paddy soil due to enhanced microbial reduction of iron and arsenic. Environ Pollut 220:514–522

Wang D, Kim BF, Nachman KE, Chiger AA, Herbstman J, Loladze I, Zhao F-J, Chen C, Gao A, Zhu Y, Li F, Shen RF, Yan X, Zhang J, Cai C, Song L, Shen M, Ma C, Yang X, Zhou W, Wang Y, Tang H, Jiang Y, Ding Y, Liu W, Sun J, Zhou W, Navas-Acien A, Zhu C, Ziska LH (2025) Impact of climate change on arsenic concentrations in paddy rice and the associated dietary health risks in Asia: an experimental and modelling study. Lancet Planet Health 9(5):e397–e409

Williams PN, Villada A, Deacon C, Raab A, Figuerola J, Green AJ, Feldmann J, Meharg AA (2007) Greatly enhanced arsenic shoot assimilation in rice leads to elevated grain levels compared to wheat and barley. Environ Sci Technol 41(19):6854–6859

Wu S, Fang GD, Wang YJ, Zheng Y, Wang C, Zhao F, Jaisi DP, Zhou DM (2017) Redox-active oxygen-containing functional groups in activated carbon facilitate microbial reduction of ferrihydrite. Environ Sci Technol 51(17):9709–9717

Wu S, Fang GD, Wang DJ, Jaisi DP, Cui PX, Wang R, Wang YJ, Wang L, Sherman DM, Zhou DM (2018) Fate of As(III) and As(V) during microbial reduction of arsenic-bearing ferrihydrite facilitated by activated carbon. ACS Earth Space Chem 2(9):878–887

Wu S, Wang D, Liu C, Fang G, Sun T-R, Cui P, Yan H, Wang Y, Zhou D (2021) Pyridinic- and pyrrolic nitrogen in pyrogenic carbon improves electron shuttling during microbial Fe(III) reduction. ACS Earth Space Chem 5(4):900–909

Xia L, Cao L, Yang Y, Ti C, Liu Y, Smith P, van Groenigen KJ, Lehmann J, Lal R, Butterbach-Bahl K, Kiese R, Zhuang M, Lu X, Yan X (2023) Integrated biochar solutions can achieve carbon-neutral staple crop production. Nat Food 4:236–246

Xin D, Li W, Choi J, Yu Y-H, Chiu PC (2023) Pyrogenic black carbon suppresses microbial methane production by serving as a terminal electron acceptor. Environ Sci Technol 57(49):20605–20614

Xu H, Hei S, Fu W, Zhang X, Liang P, Pan B, Huang X (2025) Unraveling the trade-off effect of pyrogenic carbons between biopseudocapacitors and bioconductors during anaerobic methanogenesis. Environ Sci Technol 59(5):2861–2874

Yan L, Hu S, Jing C (2016) Recent progress of arsenic adsorption on TiO_2 in the presence of coexisting ions: a review. J Environ Sci 49:74–85

Yang X, Hinzmann M, Pan H, Wang J, Bolan N, Tsang DCW, Ok YS, Wang S-L, Shaheen SM, Wang H, Rinklebe J (2022) Pig carcass-derived biochar caused contradictory effects on arsenic mobilization in a contaminated paddy soil under fluctuating controlled redox conditions. J Hazard Mater 421:126647

Yang Y, Wang Q, Xue J, Tian S, Du Y, Xie X, Gan Y, Deng Y, Wang Y (2023) Organic matter degradation and arsenic enrichment in different floodplain aquifer systems along the middle reaches of Yangtze River: a thermodynamic analysis. Water Res 239:120072

Yang J-M, Chen H-L, Wang X, Guan D-X, Ji X-H, Xie Y-H, Huang R, Peng B, Qin Q-B (2025) Toward safe rice production in As-Cd co-contaminated paddy soils: biogeochemical mechanisms and remediation strategies. Crit Rev Environ Sci Technol 55(1):1–24

Yin D, Wang X, Peng B, Tan C, Ma LQ (2017) Effect of biochar and Fe-biochar on Cd and As mobility and transfer in soil-rice system. Chemosphere 186:928–937

Yuan H-Y, Ding L-J, Zama EF, Liu P-P, Hozzein WN, Zhu Y-G (2018) Biochar modulates methanogenesis through electron syntrophy of microorganisms with ethanol as a substrate. Environ Sci Technol 52(21):12198–12207

Yuan Z-F, Zhou Y, Chen Z, Tang X, Wang Y, Kappler A, Xu J (2023a) Reduce methane emission from rice paddies by man-made aerenchymatous tissues. Carbon Res 2(1):17

Yuan Z-F, Zhou Y, Chen Z, Zhang T, Kappler A, Gustave W, Tang X, Xu J (2023b) Sustainable immobilization of arsenic by man-made aerenchymatous tissues in paddy soil. Environ Sci Technol 57(33):12280–12290

Zhang P, Zhang J, Sun Z, He C, Pan B, Xing B (2021) The conductivity and redox properties of pyrolyzed carbon mediate methanogenesis in paddy soils with ethanol as substrate. Sci Total Environ 795:148906

Zhang E, Wu S, Liu J, Li H, Liu X, Lu Y, Ge C, Zhou D (2024a) Activated carbon as a strong DOM adsorbent mitigates antimony and arsenic release in flooded mining-impacted soils. J Hazard Mater 473:134663

Zhang S, Zhang J, Niu L, Chen Q, Zhou Q, Xiao N, Man J, Ma J, Wei C, Zhang S, Luo Y, Yao Y (2024b) Escalating arsenic contamination throughout Chinese soils. Nat Sustain 7:766–775

Zhang X, Xue W, Wang G, Liang J, Wang Q, Li Y, Shu W, Zhou Q (2025) Biogeochemical coupling of C/Fe in oil-polluted wetlands associated with iron reduction. Communic Earth Environ 6(1):77

Zhao FJ, Wang P (2020) Arsenic and cadmium accumulation in rice and mitigation strategies. Plant Soil 446(1):1–21

Zhou Y, Xiao Q, Yao X, Zhang Y, Zhang M, Shi K, Lee X, Podgorski DC, Qin B, Spencer RGM, Jeppesen E (2018) Accumulation of terrestrial dissolved organic matter potentially enhances dissolved methane levels in eutrophic lake Taihu, China. Environ Sci Technol 52(18):10297–10306

Zhu C, Xue C, Huang M, Zhu F, Fang G, Wang D, Liu S, Chen N, Wu S, Zhou D (2022) Rapid As(III) oxidation mediated by activated carbons: reactive species vs. direct oxidation. Sci Total Environ 822:153536